ARTICLES
PUBLISHED ONLINE: 25 APRIL 2010 | DOI: 10.1038/NPHYS1651
nature physics

Turing patterns in network-organized activator–inhibitor systems

Hiroya Nakao[1,2]* and Alexander S. Mikhailov[3]*

Turing instability in activator–inhibitor systems provides a paradigm of non-equilibrium self-organization; it has been extensively investigated for biological and chemical processes. Turing instability should also be possible in networks, and general mathematical methods for its treatment have been formulated previously. However, only examples of regular lattices and small networks were explicitly considered. Here we study Turing patterns in large random networks, which reveal striking differences from the classical behaviour. The initial linear instability leads to spontaneous differentiation of the network nodes into activator-rich and activator-poor groups. The emerging Turing patterns become furthermore strongly reshaped at the subsequent nonlinear stage. Multiple coexisting stationary states and hysteresis effects are observed. This peculiar behaviour can be understood in the framework of a mean-field theory. Our results offer a new perspective on self-organization phenomena in systems organized as complex networks. Potential applications include ecological metapopulations, synthetic ecosystems, cellular networks of early biological morphogenesis, and networks of coupled chemical nanoreactors.

Reaction–diffusion systems support a wealth of complex self-organized patterns, such as stationary dissipative structures, travelling fronts and pulses, rotating spiral waves or chemical turbulence[1–6]. Within the last decade, attention has been brought to a class of models representing their network analogues, where the interacting species occupy network nodes and are diffusively transported across the links[7–11]. Such models typically arise when ecological metapopulations with dispersal connections between habitats are considered[12–16] or spreading of infections through transportation networks is investigated[17–21]. They can also correspond to networks of diffusively coupled chemical reactors or biological cells[8–11]. Network architecture makes the analysis of self-organization difficult, and therefore it has so far been largely restricted to such kinds of non-equilibrium pattern formation as epidemic spreading[19–21] or synchronization[22–24]. More complex forms of network self-organization are, however, also possible.

In 1952, Turing showed[1] that differences in the diffusion constants of activator and inhibitor species can bring about destabilization of the uniform state and lead to spontaneous emergence of periodic spatial patterns. The Turing patterns can emerge in autocatalytic chemical reactions with inhibition[2–4], in processes of biological morphogenesis[25–29], and in ecosystems[30–33]. They provide a classical example of complex non-equilibrium self-organization.

As early as 1971, Othmer and Scriven[8] pointed out that Turing instability can occur in network-organized systems and may play an important role in the early stages of biological morphogenesis, as morphogens diffuse over a network of intercellular connections. They have proposed a general mathematical framework for the analysis of such network instability, which has been subsequently explored[9–11]. The examples of specific applications of the theory were, however, limited to regular lattices[8,9] or small networks[10,11].

In studies of network phenomena, characteristic statistical features of collective dynamics were first revealed when large unstructured random networks, such as the Erdös–Rényi or scale-free networks[34–36], were considered, for which powerful analytical methods, for example, the mean-field approximation[19–24], can be applied. Detailed statistical investigations of the emerging stationary Turing patterns in such large random networks thus need to be performed and this is the aim of our present work.

Activator–inhibitor systems on networks

Activator–inhibitor systems in classical continuous media are described by

$$\frac{\partial}{\partial t}u(\mathbf{x},t)=f(u,v)+D_{\mathrm{act}}\nabla^2 u(\mathbf{x},t)$$

$$\frac{\partial}{\partial t}v(\mathbf{x},t)=g(u,v)+D_{\mathrm{inh}}\nabla^2 v(\mathbf{x},t) \qquad (1)$$

where $u(\mathbf{x},t)$ and $v(\mathbf{x},t)$ are local densities of the activator and inhibitor species. Functions $f(u,v)$ and $g(u,v)$ specify local dynamics of the activator, which autocatalytically enhances its own production, and of the inhibitor, which suppresses the activator growth. D_{act} and D_{inh} are the diffusion constants of activator and inhibitor species. The Turing instability[1] sets in as the ratio $D_{\mathrm{inh}}/D_{\mathrm{act}}$ of the two diffusion constants is increased and exceeds a threshold. It leads to spontaneous development of alternating activator-rich and activator-poor domains from the uniform background. The activator and the inhibitor may represent two different chemical species[2–4]. In ecological models, the activator typically corresponds to the prey and the inhibitor to the predator[5,16,30,32].

In our study, we consider the network analogue of model (1) where activator and inhibitor species occupy discrete nodes of a network and are diffusively transported over links connecting them. The links may represent diffusive connections between chemical reactors or dispersal of ecospecies from one habitat to another. The topology of a network with N nodes is defined by a symmetric adjacency matrix whose elements A_{ij} take $A_{ij}=1$ if the nodes i and j $(i,j=1,\ldots,N)$ are connected $(i\neq j)$ and $A_{ij}=0$ otherwise. The degree (number of connections) of node i is given by $k_i=\sum_{j=1}^{N}A_{ij}$. For convenience, we always sort network nodes $\{i\}$ in decreasing order of their degrees $\{k_i\}$ so that the condition $k_1\geq k_2\geq\cdots k_N$ holds. Diffusive transport of species into a certain node i is given

[1]Department of Physics, Kyoto University, Kyoto 606-8502, Japan, [2]JST, CREST, Kyoto 606-8502, Japan, [3]Department of Physical Chemistry, Fritz Haber Institute of the Max Planck Society, Faradayweg 4-6, 14195 Berlin, Germany. *e-mail: nakao@ton.scphys.kyoto-u.ac.jp; mikhailov@fhi-berlin.mpg.de.

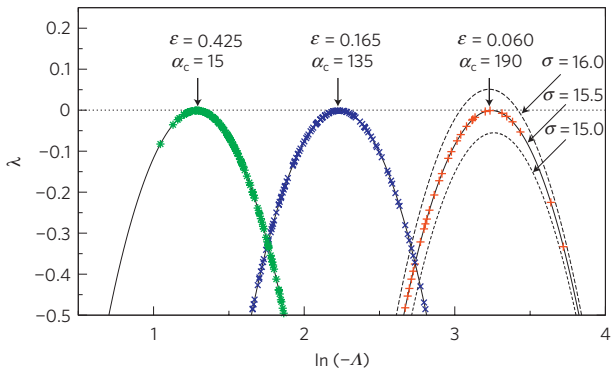

Figure 1 | Linear stability analysis. Linear growth rates λ_α of Laplacian modes $\alpha = 1, \ldots, N$ for the Mimura–Murray model on a scale-free network ($N = 200$ nodes and mean degree $\langle k \rangle = 10$) are plotted as functions of the Laplacian eigenvalues Λ_α for the critical ratio of diffusion constants $\sigma = 15.5 \simeq \sigma_c$. Three curves corresponding to three values of the diffusional mobility $\varepsilon = 0.425$, 0.165 and 0.060 are shown. For comparison, curves with $\sigma = 15.0$ and $\sigma = 16.0$ are also drawn for $\varepsilon = 0.060$. Critical modes are indicated for each value of ε. The critical modes and the corresponding Laplacian eigenvalues are $\alpha_c = 15$, $\Lambda_c = -3.62$ for $\varepsilon = 0.425$, $\alpha_c = 135$, $\Lambda_c = -9.32$ for $\varepsilon = 0.165$, and $\alpha_c = 190$, $\Lambda_c = -25.3$ for $\varepsilon = 0.060$.

by the sum of incoming fluxes to node i from other connected nodes $\{j\}$, where the fluxes are proportional to the concentration difference between the nodes (Fick's law). By introducing the network Laplacian matrix, $L_{ij} = A_{ij} - k_i\delta_{ij}$, the diffusive flux of species u to node i is expressed as $\sum_{j=1}^{N} L_{ij}u_j$, and similarly for v (see Methods section). Generally, diffusional mobilities of species u and v on a network are different.

Equations describing network-organized activator–inhibitor systems are thus given by

$$\frac{\mathrm{d}}{\mathrm{d}t}u_i(t) = f(u_i, v_i) + \varepsilon \sum_{j=1}^{N} L_{ij}u_j$$

$$\frac{\mathrm{d}}{\mathrm{d}t}v_i(t) = g(u_i, v_i) + \sigma\varepsilon \sum_{j=1}^{N} L_{ij}v_j \qquad (2)$$

for $i = 1, \ldots, N$. Now $f(u, v)$ and $g(u, v)$ represent the local activator–inhibitor dynamics on individual nodes and satisfy several conditions given in the Methods section. We denote the diffusional mobility of the activator species as $\varepsilon(=D_{\mathrm{act}})$ and that of the inhibitor species as $\sigma\varepsilon(=D_{\mathrm{inh}})$, where $\sigma = D_{\mathrm{inh}}/D_{\mathrm{act}}$ is the ratio between them. The considered systems have a uniform stationary state $(\bar{u}, \bar{v})$, where $f(\bar{u}, \bar{v}) = 0$ and $g(\bar{u}, \bar{v}) = 0$. This uniform state can become unstable because of the Turing instability.

As a particular example of an activator–inhibitor network system, the Mimura–Murray model[30] of prey–predator populations on scale-free random networks is used in the main text (see Methods section). In the Supplementary Information, results for the Brusselator model[2] and Erdös–Rényi random networks are also given.

The Turing instability

The Turing instability is revealed through linear stability analysis of the uniform stationary state with respect to non-uniform perturbations. In the classical case of continuous media[1], non-uniform perturbations are decomposed into a set of spatial Fourier modes representing plane waves with different wavenumbers. As noticed by Othmer and Scriven[8], the roles of plane waves and wavenumbers are played in networks by eigenvectors $\boldsymbol{\phi}^{(\alpha)} = (\phi_1^{(\alpha)}, \ldots, \phi_N^{(\alpha)})$ and eigenvalues Λ_α ($\alpha = 1, \ldots, N$) of their Laplacian matrices (see Methods section)[37–40].

Introducing small perturbations $(\delta u_i, \delta v_i)$ to the uniform state and substituting into equations (2), a set of coupled linearized differential equations is obtained. By expanding the perturbations over a set of Laplacian eigenvectors, $\{\boldsymbol{\phi}^{(\alpha)}\}$, the linear growth rate λ_α of each mode is determined from a characteristic equation (see Methods section). The αth mode is unstable when $\mathrm{Re}\,\lambda_\alpha$ is positive. The Turing instability occurs[8–11] when one of the modes (that is, the critical mode) begins to grow. At the instability threshold, $\mathrm{Re}\,\lambda_\alpha = 0$ for some $\alpha = \alpha_c$ and $\mathrm{Re}\,\lambda_\alpha < 0$ for all other modes.

Figure 1 shows the growth rate λ as a function of Λ for the Mimura–Murray model on a scale-free random network. Three curves, corresponding to different ratios σ of diffusion constants (below, at and above the instability threshold), are displayed for $\varepsilon = 0.06$. Critical curves for two other values of ε are also shown. The Turing instability becomes possible for $\sigma > \sigma_c$. The dispersion curve $\lambda = F(\varepsilon\Lambda)$ first touches the horizontal axis at $\Lambda = \Lambda_c$ and the Laplacian mode $\boldsymbol{\phi}^{(\alpha_c)}$, possessing the Laplacian eigenvalue Λ_{α_c} that is closest to Λ_c, becomes critical. Note that the Laplacian spectrum of a network is discrete and, therefore, the instability actually occurs only when one of the respective points on the dispersion curve crosses the horizontal axis.

The above results are analogous to those holding for continuous media (see ref. 6). The critical ratio σ_c in the networks is the same as in the classical case. The Laplacian eigenvalue Λ_c of the critical network mode corresponds to $-q_c^2$, where q_c is the critical wavenumber in the continuous media. Despite such formal analogies, properties of Turing patterns in large random networks are very different from their classical counterparts, as demonstrated in the following sections.

Critical Turing modes in large random networks

When a Turing pattern starts to grow after slightly exceeding the instability threshold, the activator and inhibitor distributions in this pattern are determined by the critical Laplacian eigenvector as $\delta u_i, \delta v_i \propto \phi_i^{(\alpha_c)}$. Therefore, to understand the organization of growing Turing patterns, the properties of Laplacian eigenvectors should be considered.

As an example, Fig. 2a,b display critical eigenvectors of a scale-free network for two different values of the diffusion constant ε. The same eigenvectors are shown graphically in Fig. 2c,d. In the chosen representation, network nodes with larger degrees (hubs) are located in the centre and the nodes with lower degrees in the periphery of the graph. The nodes are coloured red when $\phi_i^{(\alpha_c)} \geq 0.1$ (for example, the activator concentration is significantly increased), blue when $\phi_i^{(\alpha_c)} \leq -0.1$ (significantly decreased), and yellow for $-0.1 < \phi_i^{(\alpha_c)} < 0.1$ (no significant change).

It is clearly seen that spontaneous differentiation of nodes takes place—the distinguishing feature of the Turing instability. However, it affects only a fraction of all nodes. The differentiated nodes, with significant deviations of the activation level, tend to have close degrees. When diffusional mobility ε is small, only a subset of hub nodes undergoes differentiation (Fig. 2a,c). If ε is large, differentiated nodes have just a few links (Fig. 2b,d). Thus, correlation between the characteristic degrees of the differentiated nodes and the diffusional mobility exists. This behaviour is general and is related to the effect of localization of Laplacian eigenvectors.

As has recently been shown[40], Laplacian eigenvectors in large unstructured random networks with broad degree distributions tend to localize on subsets of nodes with close degrees. The localization effect for a scale-free network is illustrated in Fig. 3. Here, all nodes are divided into groups with equal degrees k. For each k and a chosen Laplacian eigenvalue Λ, the number of 'differentiated' nodes with $\phi_i^{(\alpha)} \geq 0.1$ or $\phi_i^{(\alpha)} \leq -0.1$ in the respective eigenvector $\boldsymbol{\phi}^{(\alpha)}$ is counted. The density diagrams in Fig. 3 display the relative numbers of such nodes as functions of the Laplacian eigenvalue Λ and the degree k. One can see that

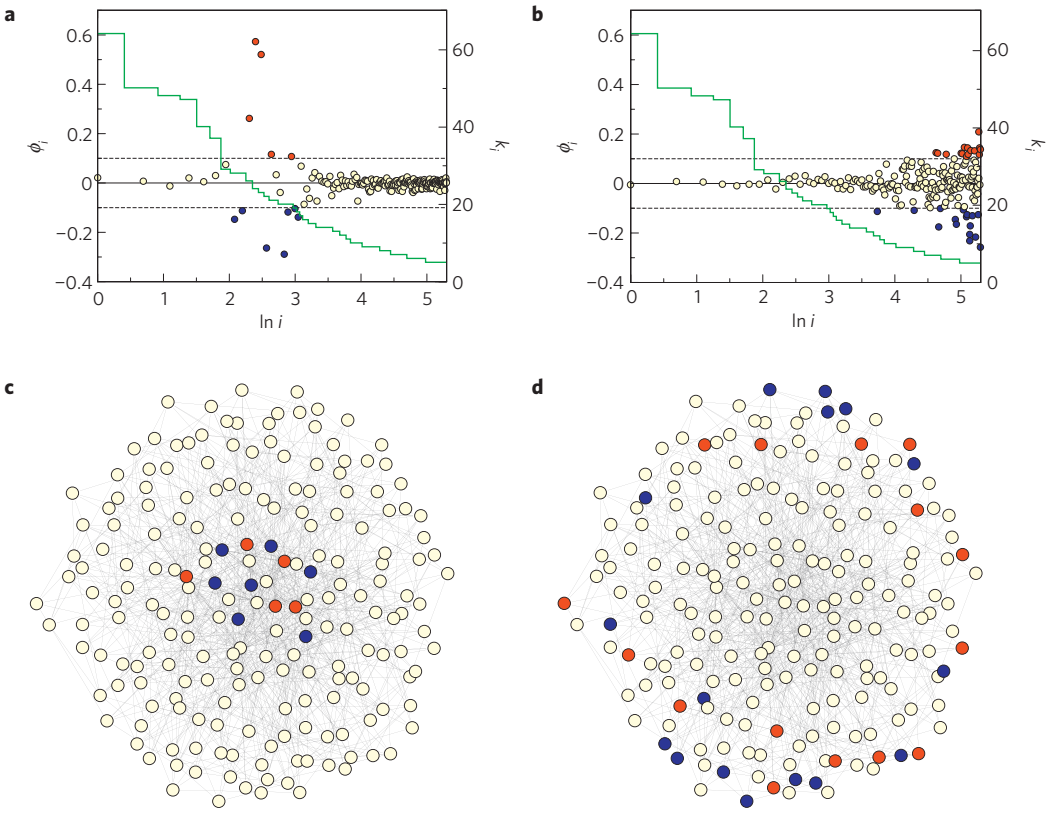

Figure 2 | Critical Turing modes of a scale-free network. The network size is $N = 200$ and the mean degree is $\langle k \rangle = 10$. **a**,**b**, Critical eigenvectors $\alpha_c = 190$ (**a**) and $\alpha_c = 15$ (**b**) plotted against the node index i. Node degrees k_i are shown by green stepwise curves. Node indices $\{i\}$ are sorted according to their degrees $\{k_i\}$. **c**,**d**, The same critical eigenvectors $\alpha_c = 190$ (**c**), and $\alpha_c = 15$ (**d**), displayed graphically on the network.

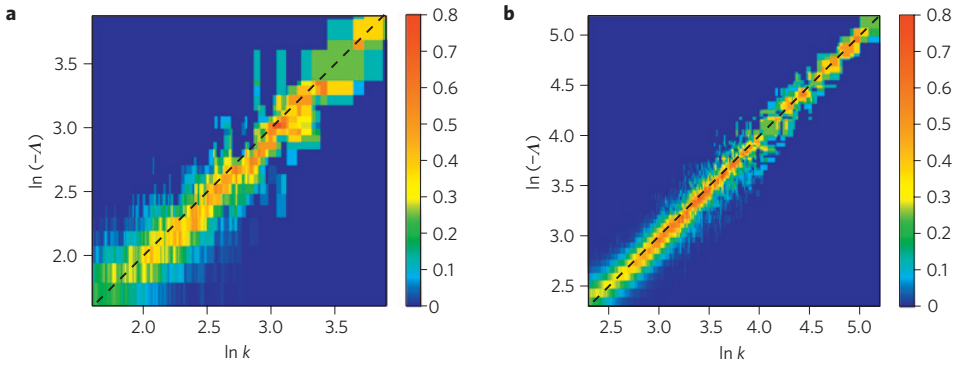

Figure 3 | Localization of Laplacian eigenvectors in scale-free networks. The network size and the mean degree are $N = 200$, $\langle k \rangle = 10$ (**a**), and $N = 1{,}000$, $\langle k \rangle = 20$ (**b**). Density distribution of differentiated nodes in each subset of nodes with equal degrees is shown for the entire set of Laplacian eigenvectors.

differentiated nodes are approximately located along the diagonal of the density map. The localization effect is more pronounced for the larger network. Thus, each Laplacian eigenvector $\boldsymbol{\phi}^{(\alpha)}$ has a characteristic localization degree $\bar{k}_\alpha$. Moreover, this characteristic degree is approximately equal to the negative of the respective eigenvalue, so that a simple relationship $\bar{k}_\alpha \simeq -\Lambda_\alpha$ holds for a scale-free network.

On the other hand, as implied by the linear stability analysis, the growth rate λ_α of each mode depends only on the combination $\varepsilon\Lambda_\alpha$ of the diffusional mobility ε and the eigenvalue Λ_α of that mode as $\lambda_\alpha = F(\varepsilon\Lambda_\alpha)$ (see Methods section). Therefore, the Laplacian eigenvalue Λ_{α_c} of the critical mode α_c with $\lambda_{\alpha_c} = 0$ should be inversely proportional to the diffusional mobility ε, that is, $\Lambda_{\alpha_c} \propto 1/\varepsilon$. Hence, modes with large negative eigenvalues Λ_α tend to become unstable for small mobilities ε (note that $\Lambda_\alpha \leq 0$ in our definition).

Combining the two relationships, $\bar{k}_\alpha \simeq -\Lambda_\alpha$ and $\Lambda_{\alpha_c} \propto 1/\varepsilon$, a simple scaling law $\bar{k}_{\alpha_c} \propto 1/\varepsilon$ is obtained. It implies that the characteristic degree $\bar{k}_{\alpha_c}$ of the differentiating subset is inversely proportional to the diffusional mobility ε. The dependence $\Lambda_{\alpha_c} \propto 1/\varepsilon$ holds for any activator–inhibitor model exhibiting the Turing instability. Similar localization of Laplacian eigenvectors is also observed for other random networks with broad degree distributions (to be separately reported). Even for Erdös–Rényi networks whose degree fluctuations should vanish in the infinite-size limit[7], finite-size degree fluctuations give rise to a certain level of localization (see Supplementary Information). The characteristic localization degree $\bar{k}_{\alpha_c}$ of the critical Turing mode is generally a

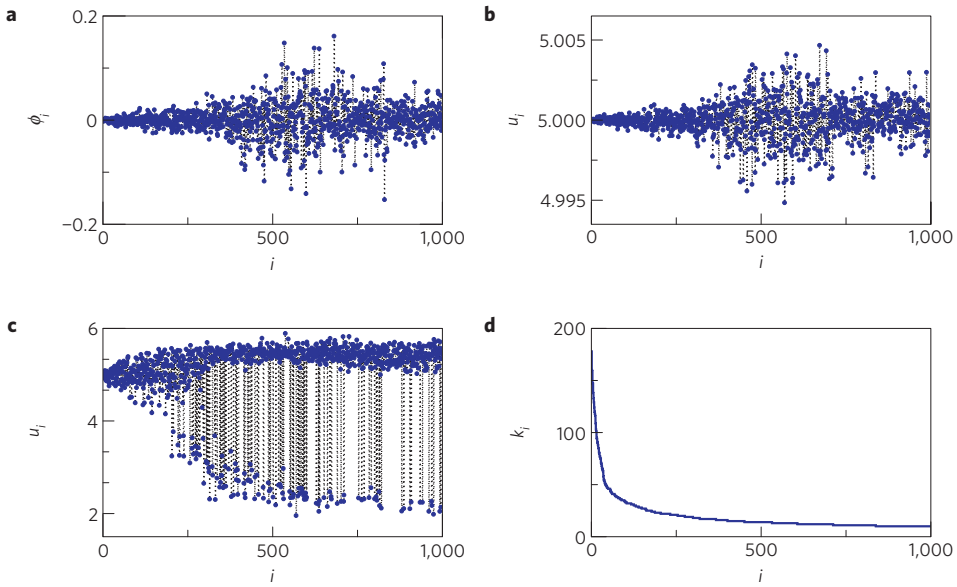

Figure 4 | Nonlinear evolution and a stationary Turing pattern. The Mimura–Murray model with parameters $\varepsilon = 0.12$ and $\sigma = 15.6$ on a scale-free network of size $N = 1,000$ and mean degree $\langle k \rangle = 20$. Nodes are ordered according to their degrees. **a**, The critical mode (the Laplacian eigenvector with $\alpha_c = 422$). **b**, The activator pattern at the early evolution stage ($t = 200$). **c**, The stationary activator pattern at the late stage ($t = 1,500$). **d**, Dependence of the degree on the node index.

monotonously increasing function of the negative of the critical Laplacian eigenvalue, $-\Lambda_{\alpha_c}$, and thus a decreasing function of the diffusional mobility ε.

Turing patterns

The initial exponential growth is followed by a nonlinear process leading to the formation of stationary Turing patterns. We have investigated nonlinear evolution of the system and properties of asymptotic stationary patterns by numerical simulations. Figure 4 presents typical results, obtained for intermediate diffusional mobility ($\varepsilon = 0.12$) and slightly above the instability threshold ($\sigma = 15.6$), for the Mimura–Murray model on a random scale-free network of size $N = 1,000$ and mean degree $\langle k \rangle = 20$. The nodes are sorted in the order of their degrees, as shown in Fig. 4d.

Starting from almost uniform initial conditions with small perturbations, exponential growth is observed at the early stage. The activator pattern at this stage, Fig. 4b, is similar to the critical mode, Fig. 4a, where the deviations result from the contributions from neighbouring modes that are already excited to some extent. Later on, however, strong nonlinear effects develop, and the final stationary pattern, Fig. 4c, becomes very different from the one determined by the critical mode.

Observing the nonlinear development, we notice that some nodes get progressively kicked off the main group near the destabilized uniform solution in this process (see Supplementary Video). Eventually, in the asymptotic stationary state, the nodes become separated into two groups. The separation occurs only for the nodes with relatively small degrees, whereas the nodes with high degrees do not differentiate.

Our numerical investigations furthermore reveal that the outcome of nonlinear evolution depends sensitively on the initial conditions. Different Turing patterns are possible at the same parameter values and strong hysteresis effects are observed. As an example, Fig. 5a shows how the amplitude of the stationary Turing pattern, defined as $A = [\sum_{i=1}^{N}\{(u_i - \bar{u})^2 + (v_i - \bar{v})^2\}]^{1/2}$, varies under gradual variation of the parameter σ in the upward or downward directions. Stationary patterns observed at points P, Q, and R in Fig. 5a are shown in Fig. 5b.

As σ was increased starting from the uniform initial condition, the Turing instability took place at $\sigma = \sigma_c$, with the amplitude A suddenly jumping up to a high value that corresponds to appearance of a kicked-off group. If σ was further increased, the amplitude A grew. Starting to decrease σ, we did not however observe a drop down at $\sigma = \sigma_c$. Instead, a punctuated decrease in the amplitude A, which is characterized by many relatively small steps, was found. Reversing the direction of change of the parameter σ at different points, many coexisting solution branches could be identified. The characteristics of Turing patterns vary with their amplitudes. When A is close to zero (point R in Fig. 5a), only a few kicked-off nodes remain in the system. Such localized Turing patterns, with only a small number of destabilized nodes, are found below the Turing instability threshold, $\sigma < \sigma_c$, and can coexist with the linearly stable uniform state.

To understand the properties of the developed Turing patterns above the instability boundary ($\sigma > \sigma_c$), one can use the mean-field approximation, similar to that previously employed for epidemic spreading models and coupled oscillators on large unstructured random networks[7,19–24,41]. In this approximation, detailed interactions of each network element with its neighbouring nodes are neglected and the element is coupled to certain global mean fields collectively determined by the entire system. The coupling strength to the global mean fields is proportional to the number of links connecting an element to the rest of the network. This approximation enables us to fit the whole stationary Turing pattern using the bifurcation diagram of an individual activator–inhibitor element coupled to global mean fields, when their values are known (see Methods section and Supplementary Information).

In Fig. 6, we compare the computed Turing patterns with the mean-field results using the values of the global mean fields yielded by direct numerical simulations. The stationary Turing patterns are well fitted by stable branches of the individual elements, although scattering of numerical data gets enhanced near the branching points. In the Supplementary Information, a similar analysis is performed for the Brusselator and for Erdös–Rényi networks. The Brusselator has a different bifurcation diagram in the presence of external fields. Nonetheless, a good agreement with the predictions of the mean-field theory is again found.

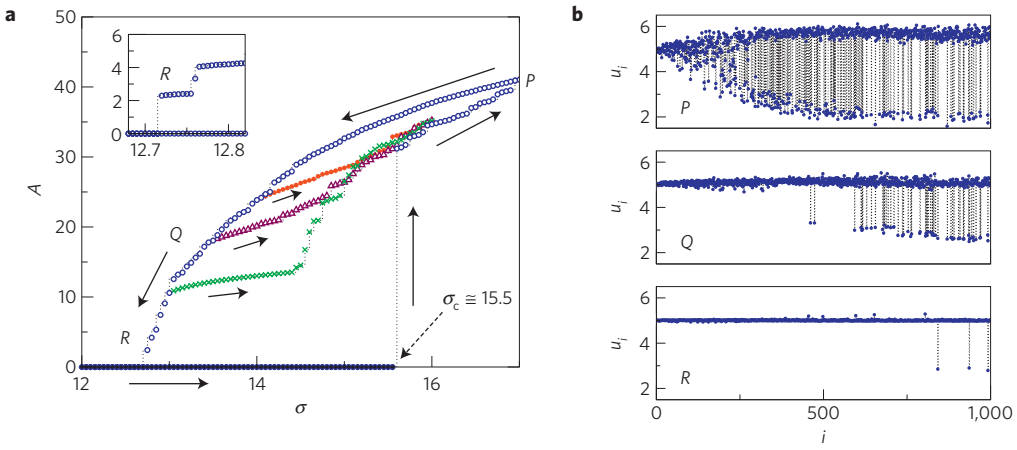

Figure 5 | Hysteresis and multistability. The Mimura–Murray model with parameters $\varepsilon = 0.12$ and $\sigma = 15.6$ on a scale-free network of size $N = 1{,}000$ and mean degree $\langle k \rangle = 20$. **a**, Amplitude A of the Turing pattern versus the diffusion ratio σ; variation directions of σ are indicated by arrows. The inset shows the blow-up near R. **b**, Stationary Turing patterns at the parameter points P ($\sigma = 17.0$), Q ($\sigma = 13.5$) and R ($\sigma = 12.8$).

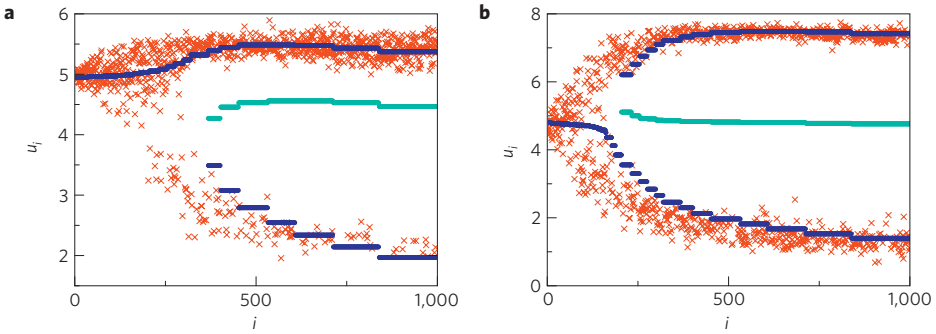

Figure 6 | Stationary Turing patterns compared with the mean-field bifurcation diagrams. The Mimura–Murray model on a scale-free network of size $N = 1{,}000$ and mean degree $\langle k \rangle = 20$. The diffusion ratio is $\sigma = 15.6$ (**a**), and $\sigma = 30$ (**b**). The diffusional mobility $\varepsilon = 0.12$ is fixed. Crosses show computed Turing patterns. Blue curves (dots) indicate stable branches and light-blue curves (dots) correspond to unstable branches of a single activator–inhibitor system coupled to the global mean fields. See Supplementary Information for details.

Thus, fully developed network Turing patterns are essentially explained by the bifurcation diagrams of a single node coupled to the global mean fields, with the coupling strength determined by the degree of the respective network node. The mean-field theory is generally not applicable for localized Turing patterns below the Turing instability threshold.

Discussion

The fingerprint property of the classical Turing instability in continuous media is the spontaneous formation of periodic stationary patterns. Our investigations of the Turing problem for large random networks have revealed that, whereas the bifurcation remains essentially the same, properties of emergent patterns are very different. In networks, the critical Turing mode is approximately localized on a subset of nodes with their degrees close to some characteristic value controlled by the mobility of species. The final stationary patterns deviate strongly from the critical mode. Multistability, that is, coexistence of a number of different stationary patterns for the same parameter values, is typically found and hysteresis phenomena are observed. As we have shown, fully developed network Turing patterns above the instability threshold can be well understood within the mean-field approximation.

The origins of such difference lie in the statistical structural properties of network-organized systems. The diameters of random networks are typically small (at most $L = \ln N$ for random scale-free networks[42]). Because of their small diameters, diffusional mixing in such systems is fast, explaining why the mean-field approximation works so well there. For comparison, a d-dimensional cubic lattice with N nodes has a diameter of about $L = N^{1/d}$. Thus, a lattice with the same number N of nodes and a comparable diameter L should have a high dimension $d \gg 1$. Large random networks are thus structurally much closer to high-dimensional lattices or globally coupled systems than to the lattices with a few dimensions. Because of their small diameters, Turing patterns with alternating domains cannot exist in such systems, and only several domains (clusters) may be present there, as indeed seen by us for the considered networks. Note that spontaneous differentiation of elements into two groups has been previously observed in studies of globally coupled activator–inhibitor systems[43,44].

There is, however, a further important aspect distinguishing complex networks from high-dimensional lattices and globally coupled systems, namely, strong degree heterogeneity. It plays a significant role in problems involving network diffusion. Indeed, under the same concentration gradients across the links, a node with a higher number of links receives a larger incoming flux from the neighbouring nodes and also more strongly influences the rest of the system. Approximate localization of the Laplacian eigenvectors on the subsets of nodes with close degrees is characteristic for such networks[40]. It is also known that the exact localization of Laplacian eigenvectors can occur on networks[11]. However, it is only possible for networks having special structures and, typically, it would not be found in large random networks.

In contrast to scale-free networks, all nodes in an Erdös–Rényi network become statistically identical in the infinite-size limit and the heterogeneity disappears[7]. Therefore, Turing patterns in such networks should tend to become uniformly random in this limit, similar to those in globally coupled systems[43,44]. Note, however, that significant heterogeneity and, thus, localization are still found by us for Erdös–Rényi networks with about a thousand of nodes, viewed as large in typical biological or ecological applications.

Turing instability may be realized experimentally using networks of coupled chemical reactors[10]. Recent progress in nanofluidics allows one to construct even microscopical biomimetic reactors, down to the nanoscale, and couple many of them into complex networks[45]. The original study by Othmer and Scriven[8] has been motivated by an observation that, in the early stages of biological morphogenesis, an embryo should represent a multicellular network rather than a continuous reaction–diffusion medium. Indeed, the contact network of biological cells in the developing embryo of *Caenorhabditis elegans* has been determined[46,47] and much experimental evidence for the presence of activator–inhibitor mechanisms in biological morphogenesis has been gathered[26–29]. Turing instability may occur in cellular networks under the same conditions as those for continuous biological media.

There has long been discussion about the possibility of classical Turing patterns in spatially extended ecological systems. Recently, it has been shown that the conditions needed for the Turing instability in predator–prey ecosystems can be generally satisfied and, therefore, Turing patterns should represent a characteristic form of ecological self-organization[31–33]. There is a broad class of ecological systems which represent networks[12–16]. The nodes of such a network are individual habitat patches (such as trees or lakes), and diffusive coupling between them results from dispersal connections between the habitats. Complex networks of connections between the habitats can develop (see, for example, refs 13–15). Often, predators are more mobile than the prey, thus favouring the Turing instability. Similar behaviour may be expected in epidemiology where infected individuals are autocatalytically reproducing and the number of available susceptible individuals may get reduced, decreasing the reproduction efficiency[5]. Spreading of infections over air transportation networks has been actively discussed[7,17,18].

Taking into account that preconditions for the Turing instability are satisfied by a broad class of biological and ecological systems, it is very possible that such an instability has already been observed in experiments. However, it would be difficult to tell, by looking at species distribution, whether a particular observed complex pattern is a result of an intrinsic Turing instability or it is a consequence of heterogeneity in the local properties of the nodes. In this situation, an efficient strategy may be to focus not merely on the observation of complex patterns, but to investigate how such patterns respond to various perturbations and parameter variations. Such a strategy has recently been successfully followed to prove the existence of the classical Turing instability in the patterns of skin colouring in fish[48,49]. If an observed pattern is the result of the Turing mechanism, it should develop spontaneously when the conditions are changed. Only a subset of network nodes which have similar degrees should undergo differentiation initially and this subset would change for the same network if the mobilities of species or other parameters are varied. After a perturbation, a different stable stationary pattern should generally be established.

It has already been demonstrated[50] that synthetic predator–prey ecosystems can be experimentally designed. If such a system is distributed over a number of habitats with artificial dispersal connections between the habitats and, moreover, if the rates of dispersal for the predator and the prey species can be independently controlled, this would present a clear set-up for the experimental investigations of Turing patterns in ecological networks.

Methods

Model. As u is the activator and v is the inhibitor in equation (2), the partial derivatives of $f(u,v)$ and $g(u,v)$ at $(\bar{u},\bar{v})$ should satisfy the following conditions: $f_u=\partial f/\partial u|_{(\bar{u},\bar{v})}>0$, $f_v=\partial f/\partial u|_{(\bar{u},\bar{v})}<0$, $g_u=\partial g/\partial u|_{(\bar{u},\bar{v})}>0$, and $g_v=\partial g/\partial v|_{(\bar{u},\bar{v})}<0$. The uniform stationary state of the system $(u_i,v_i)=(\bar{u},\bar{v})$ for all $i=1,\ldots,N$ is assumed to be linearly stable in the absence of diffusion, which requires $f_u+g_v<0$ and $f_ug_v-f_vg_u>0$.

In the Mimura–Murray model[30], u and v correspond to prey and predator densities. In this model, we have $f(u,v)=\{(a+bu-u^2)/c-v\}u$ and $g(u,v)=\{u-(1+dv)\}v$, where the parameters have been chosen as $a=35$, $b=16$, $c=9$, and $d=2/5$ in the present study, yielding the fixed point $(\bar{u},\bar{v})=(5,10)$.

Scale-free networks were generated by the preferential attachment algorithm of Barábasi and Albert[34,36], in which nodes with larger degrees tend to acquire more links. Starting from m fully connected initial nodes, we added m new connections at each iteration step, so that the mean degree is $\langle k\rangle\simeq 2m$.

Network Laplacian matrix. The Laplacian L_{ij} of a network is a real, symmetric, and negative semi-definite matrix, whose elements are given by $L_{ij}=A_{ij}-k_i\delta_{ij}$, where $k_i=\sum_{j=1}^{N}A_{ij}$ is the degree of the node i. Diffusive flux of the species u to node i is expressed as $\sum_{j=1}^{N}L_{ij}u_j=\sum_{j=1}^{N}A_{ij}(u_j-u_i)$, and similarly for v.

The eigenvalues Λ_α and eigenvectors $\boldsymbol{\phi}^{(\alpha)}=(\phi_1^{(\alpha)},\ldots,\phi_N^{(\alpha)})$ of the Laplacian matrix L_{ij} are determined by $\sum_{j=1}^{N}L_{ij}\phi_j^{(\alpha)}=\Lambda_\alpha\phi_i^{(\alpha)}$, with $\alpha=1,\ldots,N$. All eigenvalues of L_{ij} are real and non-positive. We sort the indices $\{\alpha\}$ in decreasing order of the eigenvalues, so that the condition $0=\Lambda_1\geq\Lambda_2\geq\cdots\geq\Lambda_N$ holds. The eigenvectors are orthonormalized as $\sum_{i=1}^{N}\phi_i^{(\alpha)}\phi_i^{(\beta)}=\delta_{\alpha,\beta}$ where $\alpha,\beta=1,\ldots,N$.

Linear stability analysis. The linear stability analysis is performed in close analogy to the classical case of continuous media. We introduce small perturbations δu_i and δv_i to the uniform state as $(u_i,v_i)=(\bar{u},\bar{v})+(\delta u_i,\delta v_i)$ and substitute this into equation (2). Linearized differential equations for δu_i and δv_i are obtained as $\mathrm{d}\delta u_i/\mathrm{d}t=f_u\delta u_i+f_v\delta v_i+\varepsilon\sum_{j=1}^{N}L_{ij}\delta u_j$ and $\mathrm{d}\delta v_i/\mathrm{d}t=g_u\delta u_i+g_v\delta v_i+\sigma\varepsilon\sum_{j=1}^{N}L_{ij}\delta v_j$. By expanding the perturbations δu_i and δv_i over the set of Laplacian eigenvectors as $\delta u_i(t)=\sum_{\alpha=1}^{N}c_\alpha\exp[\lambda_\alpha t]\phi_i^{(\alpha)}$ and $\delta v_i(t)=\sum_{\alpha=1}^{N}c_\alpha B_\alpha\exp[\lambda_\alpha t]\phi_i^{(\alpha)}$, these equations are transformed into N independent linear equations for different normal modes, resulting in the following eigenvalue equation for each α:

$$\lambda_\alpha\begin{pmatrix}1\\B_\alpha\end{pmatrix}=\begin{pmatrix}f_u+\varepsilon\Lambda_\alpha & f_v\\ g_u & g_v+\sigma\varepsilon\Lambda_\alpha\end{pmatrix}\begin{pmatrix}1\\B_\alpha\end{pmatrix}$$

Note that the Laplacian eigenvalue Λ_α appears here only in combination with the diffusional mobility ε in the form $\varepsilon\Lambda_\alpha$. From the characteristic equation $\{\lambda_\alpha-f_u-\varepsilon\Lambda_\alpha\}\{\lambda_\alpha-g_v-\sigma\varepsilon\Lambda_\alpha\}-f_vg_u=0$, a pair of conjugate growth rates is obtained for each Laplacian mode as $\lambda_\alpha=(1/2)\{f_u+g_v+(1+\sigma)\varepsilon\Lambda_\alpha\pm[4f_vg_u+(f_u-g_v+(1-\sigma)\varepsilon\Lambda_\alpha)^2]^{1/2}\}$. Only the upper branch can become positive, and it is always chosen as λ_α in our analysis. From the condition that λ_α touches the horizontal axis at its maximum, the critical value of σ is determined as $\sigma_c=\{f_ug_v-2f_vg_u+2[f_vg_u(f_vg_u-f_ug_v)]^{1/2}\}/f_u^2$. The critical Laplacian eigenvalue is determined for a given ε as $\Lambda_c=\{(f_u-g_v)\sigma_c-\sqrt{|f_v|g_u\sigma_c}(\sigma_c+1)\}/\{\varepsilon\sigma_c(\sigma_c-1)\}$. In the Turing instability, the critical mode is not oscillatory, $\mathrm{Im}\,\lambda_{\alpha_c}=0$. The critical eigenvector in the (u,v) plane is given by $(1,B_c)$, where $B_c=\{-f_u+g_v+(\sigma_c-1)\varepsilon\Lambda_c+[4f_vg_u+(f_u-g_v-(\sigma_c-1)(\varepsilon\Lambda_c))^2]^{1/2}\}/(2f_v)$. This B_c is positive, and thus when the activator concentration increases, the inhibitor concentration also increases accordingly. These expressions coincide with the respective expressions for the continuous media[6], if we replace Λ by $-q^2$, where q is the wavenumber of the plane wave mode.

Mean-field approximation. We start by writing equation (2) in the form $\mathrm{d}u_i/\mathrm{d}t=f(u_i,v_i)+\varepsilon(h_i^{(u)}-k_iu_i)$ and $\mathrm{d}v_i/\mathrm{d}t=g(u_i,v_i)+\sigma\varepsilon(h_i^{(v)}-k_iv_i)$, where local fields felt by each node, $h_i^{(u)}=\sum_{j=1}^{N}A_{ij}u_j$ and $h_i^{(v)}=\sum_{j=1}^{N}A_{ij}v_j$, are introduced. These local fields are then approximated as $h_i^{(u)}\simeq k_iH^{(u)}$ and $h_i^{(v)}\simeq k_iH^{(v)}$, where global mean fields are defined by $H^{(u)}=\sum_{j=1}^{N}w_ju_j$ and $H^{(v)}=\sum_{j=1}^{N}w_jv_j$. The weights $w_j=k_j/(\sum_{\ell=1}^{N}k_\ell)=k_j/k_{\mathrm{total}}$ take into account the difference in contributions of different nodes to the global mean field, depending on their degrees (refs 19,22,41).

With this approximation, the individual activator–inhibitor system on each node interacts only with the global mean fields $H^{(u)}$ and $H^{(v)}$ and its dynamics is described by

$$\frac{\mathrm{d}}{\mathrm{d}t}u(t)=f(u,v)+\beta(H^{(u)}-u)$$

$$\frac{\mathrm{d}}{\mathrm{d}t}v(t)=g(u,v)+\sigma\beta(H^{(v)}-v)\qquad(3)$$

We have dropped here the index i, as all nodes obey the same equations, and introduced the parameter $\beta(i)=\varepsilon k_i$. If the diffusion ratio σ is fixed and the global mean fields $H^{(u)}$ and $H^{(v)}$ are given, the parameter β plays the role of a bifurcation parameter that controls the dynamics of each node. Equation (3)

has a single stable fixed point when $\beta = 0$ (that is, $\varepsilon = 0$), and, as β is increased, this system typically undergoes a saddle-node bifurcation that gives rise to a new stable fixed point.

In Fig. 6, we have computed stationary Turing patterns of the Mimura–Murray model by numerical integration of equation (2), and determined the respective global mean fields $H^{(u)}$ and $H^{(v)}$ at $\sigma = 15.6$ and $\sigma = 30$. Substituting these computed global mean fields into equation (3), bifurcation diagrams of a single node have been obtained. Each node i in the network is characterized by its degree k_i, so that it possesses a certain value of the bifurcation parameter, $\beta = \varepsilon k_i$. Therefore, the obtained bifurcation diagrams can be projected onto the Turing pattern as shown in Fig. 6. See Supplementary Information for more details.

Received 23 December 2008; accepted 15 March 2010; published online 25 April 2010

References

1. Turing, A. M. The chemical basis of morphogenesis. *Phil. Trans. R. Soc. Lond. B* **237,** 37–72 (1952).
2. Prigogine, I. & Lefever, R. Symmetry breaking instabilities in dissipative systems. II. *J. Chem. Phys.* **48,** 1695–1700 (1968).
3. Castets, V., Dulos, E., Boissonade, J. & De Kepper, P. Experimental evidence of a sustained standing Turing-type nonequilibrium chemical pattern. *Phys. Rev. Lett.* **64,** 2953–2956 (1990).
4. Ouyang, Q. & Swinney, H. L. Transition from a uniform state to hexagonal and striped Turing patterns. *Nature* **352,** 610–612 (1991).
5. Murray, J. D. *Mathematical Biology* (Springer, 2003).
6. Mikhailov, A. S. *Foundations of Synergetics I. Distributed Active Systems* 2nd revised edn (Springer, 1994).
7. Barrat, A., Barthélemy, M. & Vespignani, A. *Dynamical Processes on Complex Networks* (Cambridge Univ. Press, 2008).
8. Othmer, H. G. & Scriven, L. E. Instability and dynamic pattern in cellular networks. *J. Theor. Biol.* **32,** 507–537 (1971).
9. Othmer, H. G. & Scriven, L. E. Nonlinear aspects of dynamic pattern in cellular networks. *J. Theor. Biol.* **43,** 83–112 (1974).
10. Horsthemke, W., Lam, K. & Moore, P. K. Network topology and Turing instability in small arrays of diffusively coupled reactors. *Phys. Lett. A* **328,** 444–451 (2004).
11. Moore, P. K. & Horsthemke, W. Localized patterns in homogeneous networks of diffusively coupled reactors. *Physica D* **206,** 121–144 (2005).
12. Hanski, I. Metapopulation dynamics. *Nature* **396,** 41–49 (1998).
13. Urban, D. & Keitt, T. Landscape connectivity: A graph-theoretic perspective. *Ecology* **82,** 1205–1218 (2001).
14. Fortuna, M. A., Gómez-Rodrǵuez, C. & Bascompte, J. Spatial network structure and amphibian persistence in stochastic environments. *Proc. R. Soc. B* **273,** 1429–1434 (2006).
15. Minor, E. S. & Urban, D. L. A graph-theory framework for evaluating landscape connectivity and conservation planning. *Conserv. Biol.* **22,** 297–307 (2008).
16. Holland, M. D. & Hastings, A. Strong effect of dispersal network structure on ecological dynamics. *Nature* **456,** 792–795 (2008).
17. Hufnagel, L., Brockmann, D. & Geisel, T. Forecast and control of epidemics in a globalized world. *Proc. Natl Acad. Sci. USA* **101,** 15124–15129 (2004).
18. Colizza, V., Barrat, A., Barthélemy, M. & Vespignani, A. The role of the airline transportation network in the prediction and predictability of global epidemics. *Proc. Natl Acad. Sci.* **103,** 2015–2020 (2006).
19. Pastor-Satorras, R. & Vespignani, A. Epidemic spreading in scale-free networks. *Phys. Rev. Lett.* **86,** 3200–3203 (2001).
20. Colizza, V., Pastor-Satorras, R. & Vespignani, A. Reaction–diffusion processes and metapopulation models in heterogeneous networks. *Nature Phys.* **3,** 276–282 (2007).
21. Colizza, V. & Vespignani, A. Epidemic modeling in metapopulation systems with heterogeneous coupling pattern: Theory and simulations. *J. Theor. Biol.* **251,** 450–467 (2008).
22. Ichinomiya, T. Frequency synchronization in a random oscillator network. *Phys. Rev. E* **70,** 026116 (2004).
23. Boccaletti, S., Latora, V., Moreno, Y., Chavez, M. & Hwang, D-U. Complex networks: Structure and dynamics. *Phys. Rep.* **424,** 175–308 (2006).
24. Arenas, A., Díaz-Guilera, A., Kurths, J., Moreno, Y. & Zhou, C. Synchronization in complex networks. *Phys. Rep.* **469,** 93–153 (2008).
25. Meinhardt, H. & Gierer, A. Pattern formation by local self-activation and lateral inhibition. *BioEssays* **22,** 753–760 (2000).
26. Harris, M. P., Williamson, S., Fallon, J. F., Meinhardt, H. & Prum, R. O. Molecular evidence for an activator–inhibitor mechanism in development of embryonic feather branching. *Proc. Natl Acad. Sci. USA* **102,** 11734–11739 (2005).
27. Maini, P. K., Baker, R. E. & Chuong, C. M. The Turing model comes of molecular age. *Science* **314,** 1397–1398 (2006).
28. Newman, S. A. & Bhat, R. Activator–inhibitor dynamics of vertebrate limb pattern formation. *Birth Defects Res. (Part C)* **81,** 305–319 (2007).
29. Miura, T. & Shiota, K. TGFβ2 acts as an 'activator' molecule in reaction–diffusion model and is involved in cell sorting phenomenon in mouse limb micromass culture. *Dev. Dyn.* **217,** 241–249 (2000).
30. Mimura, M. & Murray, J. D. Diffusive prey–predator model which exhibits patchiness. *J. Theor. Biol.* **75,** 249–262 (1978).
31. Maron, J. L. & Harrison, S. Spatial pattern formation in an insect host-parasitoid system. *Science* **278,** 1619–1621 (1997).
32. Baurmann, M., Gross, T. & Feudel, U. Instabilities in spatially extended predator–prey systems: Spatio-temporal patterns in the neighborhood of Turing–Hopf bifurcations. *J. Theor. Biol.* **245,** 220–229 (2007).
33. Rietkerk, M. & van de Koppel, J. Regular pattern formation in real ecosystems. *Trends Ecol. Evolut.* **23,** 169–175 (2008).
34. Barabási, A-L. & Albert, R. Emergence of scaling in random networks. *Science* **286,** 509–512 (1999).
35. Strogatz, H. S. Exploring complex networks. *Nature* **410,** 268–276 (2001).
36. Albert, R. & Barabási, A-L. Statistical mechanics of complex networks. *Rev. Mod. Phys.* **74,** 47–97 (2002).
37. Dorogovtsev, S. N., Goltsev, A. V., Mendes, J. F. F. & Samukhin, A. N. Spectra of complex networks. *Phys. Rev. E* **68,** 046109 (2003).
38. Kim, D-H. & Motter, A. E. Ensemble averageability in network spectra. *Phys. Rev. Lett.* **98,** 248701 (2007).
39. Samukhin, A. N., Dorogovtsev, S. N. & Mendes, J. F. F. Laplacian spectra of, and random walks on, complex networks: Are scale-free architectures really important? *Phys. Rev. E* **77,** 036115 (2008).
40. McGraw, P. N. & Menzinger, M. Laplacian spectra as a diagnostic tool for network structure and dynamics. *Phys. Rev. E* **77,** 031102 (2008).
41. Nakao, H. & Mikhailov, A. S. Diffusion-induced instability and chaos in random oscillator networks. *Phys. Rev. E* **79,** 036214 (2009).
42. Cohen, R. & Havlin, S. Scale-free networks are ultrasmall. *Phys. Rev. Lett.* **90,** 058701 (2003).
43. Mizuguchi, T. & Sano, M. Proportion regulation of biological cells in globally coupled nonlinear systems. *Phys. Rev. Lett.* **75,** 966–969 (1995).
44. Nakajima, A. & Kaneko, K. Regulative differentiation as bifurcations of interacting cell population. *J. Theor. Biol.* **253,** 779–787 (2008).
45. Karlsson, A. *et al.* Molecular engineering: Networks of nanotubes and containers. *Nature* **409,** 150–152 (2001).
46. Bignone, F. A. Structural complexity of early embryos: A study on the nematode Caenorhabditis elegans. *J. Biol. Phys.* **27,** 257–283 (2001).
47. Schnabel, R. *et al.* Global cell sorting in the *C. elegans* embryo defines a new mechanism for pattern formation. *Dev. Biol.* **294,** 418–431 (2006).
48. Kondo, S. & Asai, R. A reaction–diffusion wave on the skin of the marine angelfish Pomacanthus. *Nature* **376,** 765–768 (1995).
49. Nakamasu, A., Takahashi, G., Kanbe, A. & Kondo, S. Interactions between zebrafish pigment cells responsible for the generation of Turing patterns. *Proc. Natl Acad. Sci. USA* **106,** 8429–8434 (2009).
50. Balagaddé, F. K. *et al.* A synthetic Escherichia coli predator–prey ecosystem. *Mol. Syst. Biol.* **4,** 1–8 (2008).

Acknowledgements

This work was supported by the Volkswagen Foundation, Germany, and by the MEXT, Japan (Global COE Program 'The Next Generation of Physics, Spun from Universality and Emergence' and Kakenhi Grant No. 19760253).

Author contributions

Both authors designed the study, carried out the analysis, and contributed to writing the paper. H.N. performed numerical simulations.

Additional information

The authors declare no competing financial interests. Supplementary information accompanies this paper on www.nature.com/naturephysics. Reprints and permissions information is available online at http://npg.nature.com/reprintsandpermissions. Correspondence and requests for materials should be addressed to H.N. or A.S.M